



Estimating Near-Surface Shear-Wave-Velocity Structures Via Multichannel Analysis of Rayleigh and Love Waves: An Experiment at the Boise Hydrogeophysical Research Site

Binbin Mi¹ · Jianghai Xia¹ · John H. Bradford² · Chao Shen³

Received: 24 May 2019 / Accepted: 23 December 2019 / Published online: 3 January 2020
© Springer Nature B.V. 2020

Abstract

Surface-wave analysis has been widely used for near-surface geophysical and geotechnical studies by using the dispersive characteristic of surface waves (Rayleigh or Love waves) to determine subsurface model parameters. Unlike Rayleigh waves, the dispersive nature of Love waves is independent of P-wave velocity in 1D models, which makes Love-wave dispersion curve interpretation simpler than Rayleigh waves. This reduces the degree of non-uniqueness leading to more stable inversion of Love-wave dispersion curves. To estimate the near-surface shear-wave velocities (V_s) using multichannel analysis of Rayleigh (MASW) and Love waves (MALW) for hydrologic characterization, we conducted an experiment at the Boise Hydrogeophysical Research Site (BHRS, an experimental well field located near Boise, Idaho, USA). We constructed the pseudo-3D velocity structures at the BHRS using both the MASW and MALW methods and compared the results to borehole measurements. We used the 3D V_s distribution to identify and resolve the extent of a relatively low-velocity anomaly caused by a sand channel. The V_s structure and anomaly boundaries were delineated at the meter scale and confirmed by the ground-penetrating radar surveys. The differences in shear-wave velocity determined by MASW, MALW and borehole measurements were discussed and interpreted to reflect the near-surface anisotropy associated with the hydrologic characteristics at the BHRS. Our results demonstrated that the combination of MALW and MASW can be a powerful tool for near-surface characterization.

Keywords MASW · MALW · Near-surface V_s structure · Anomaly delineation · Anisotropy

✉ Jianghai Xia
jianghai_xia@yahoo.com; jhxia@zju.edu.cn

¹ School of Earth Sciences, Zhejiang University, 38 Zheda Road, Hangzhou 310027, Zhejiang, China

² Department of Geophysics, Colorado School of Mines, 1500 Illinois St, Golden, CO 80401, USA

³ College of Metrology and Measurement Engineering, China Jiliang University, 258 Xueyuan Street, Hangzhou 310018, Zhejiang, China

1 Introduction

The reconstruction of near-surface elastic parameter models is of fundamental importance in near-surface geophysical investigations. Surface waves dominate the shallow-seismic wavefield and are usually characterized by being relatively low velocity, low frequency, high amplitude, and dispersive (Sheriff 2002). Surface-wave analysis provides an alternative way to identify model parameters by using the dispersive nature of surface waves. It has been widely used for near-surface geophysical and geotechnical studies over the last two decades (e.g., Socco et al. 2010; Xia 2014).

Surface-wave analysis for near-surface applications started with the spectral analysis of surface waves (SASW; Nazarian and Stokoe 1984) and grew in popularity after the introduction of the multichannel analysis of surface waves (MASW) method (Song et al. 1989; Xia et al. 1999; Park et al. 1999; Miller et al. 1999). The conventional MASW method was originally developed to estimate the near-surface shear (S) wave velocity distribution from high-frequency (≥ 2 Hz) vertical component Rayleigh-wave dispersion data with an active source. Compared to SASW, the MASW method greatly improves the accuracy and efficiency of surface-wave surveys by the use of multiple receivers (e.g., Lin et al. 2017). MASW mainly consists of three steps: (1) acquire high-frequency broadband Rayleigh waves using a multichannel recording system, (2) extract dispersion curves of Rayleigh waves, and then (3) invert Rayleigh-wave dispersion curves for near-surface S-wave velocity (V_s) profiles. S-wave velocities determined by MASW have been reliably and successfully correlated with borehole data (e.g., Miller et al. 1999; Xia et al. 2002; Foti et al. 2011; Fiore et al. 2016; Garofalo et al. 2016).

The correct estimation and identification of multimodal dispersion curves is one of the key steps of using surface-wave methods to obtain S-wave velocities. This task is not straightforward because some modes may not be present in the experimental data and very smooth changes from one mode to another (mode kissing or osculation) may occur, especially in environments with strong velocity contrasts (Boaga et al. 2013; Gao et al. 2016) and low-velocity layers (Mi et al. 2018). The misidentification of modes may produce significant errors in inversion (Zhang and Chan 2003). The inverted S-wave velocity profile represents an average of the structure below the recording array, which is based on the assumption of a horizontally layered earth model (Xia et al. 1999). The lateral variations are finally retrieved by merging 1D velocity profiles to reconstruct 2D velocity structures (e.g., Miller et al. 1999; Xia et al. 2004). The horizontal resolution of the MASW method is influenced by the parameters of the recording system, and the receiver spread length used to extract dispersion curves sets the theoretical lower limit (Mi et al. 2017).

For an overview of high-frequency surface-wave methods, we refer the reader to Socco et al. (2010), Foti et al. (2011), Xia (2014) and Mi et al. (2018) for the latest developments. Pan et al. (2019) present a comprehensive review and comparison of MASW and shallow-seismic full waveform inversion (FWI). Both MASW and FWI provide ways to use shallow-seismic surface waves in reconstructing near-surface structures. FWI has a high nonlinearity and resolution, whereas MASW possesses a relatively low resolution but increased inversion stability and low-cost (Pan et al. 2019). Many efforts have been made during the past two decades to improve the accuracy and resolution of the MASW method, especially in areas with complex near-surface structures (e.g., Beaty et al. 2002; Socco and Strobbia 2003; Forbriger 2003; Xia et al. 2003; Hayashi and Suzuki 2004; Strobbia and Foti 2006; Lin and Lin 2007; Boiero and Socco 2010; Vignoli et al. 2011; Bergamo et al. 2012; Ikeda et al. 2013; Wang et al. 2015; Yin et al. 2016; Ning et al. 2018).

Commonly the MASW method uses the vertical component data of Rayleigh waves in near-surface applications. Multicomponent data can provide more information on the model parameters (Mi et al. 2019) due to the different dispersion energy distribution (Boaga et al. 2013; Ikeda et al. 2015; Qiu et al. 2019). Love waves are formed by constructive interference of multiple reflections of SH waves, which can be recorded by horizontal component geophones along the free surface. Unlike Rayleigh waves, Love waves are independent of P-wave velocity in 1D models. The dispersion curves of Love waves are simpler to interpret than Rayleigh waves and the phenomenon of “mode kissing” is less common in dispersion images of Love-wave energy (Xia et al. 2012). The independence of P-wave velocity reduces the degree of nonuniqueness and makes the inversion of Love-wave dispersion curves more stable (Xia et al. 2012). Based on these advantages, the multichannel analysis of Love waves (MALW) has received increased attention in recent years (e.g., Xia et al. 2012; Mi et al. 2015; Dal Moro et al. 2015). The combined use of MASW and MALW may avoid mode misidentification and provide more reliable results.

S-wave velocities inferred from Rayleigh waves (vertically polarized shear (SV) wave velocities, V_{SV}) often differ from those derived from Love waves (horizontally polarized shear (SH) wave velocities, V_{SH}). Such incompatibilities are generally considered as an evidence for the presence of anisotropy, commonly addressed as radial or polarization anisotropy (e.g., Anderson 1961; Muzyert and Snieder 2000). The difference in S-wave velocities derived from Rayleigh and Love waves has been widely used to determine the anisotropy in the crust and upper mantle (e.g., Lin et al. 2008; Cheng et al. 2013; Luo et al. 2013; Yuan and Beghein, 2014). On the near-surface anisotropy, however, few cases have been investigated using MASW and MALW.

The MASW method has been applied to a wide range of problems in geotechnical and environmental engineering, such as mapping bedrock (Miller et al. 1999), delineating shallow fault zones (Ivanov et al. 2006; Yilmaz et al. 2006; Ikeda et al. 2013), detecting voids (Xia et al. 2004, 2005; Sloan et al. 2015; Schwenk et al. 2016), and assessing landslide stability (Mi et al. 2017). The applications of MALW are rarely implemented due to the limitation of Love-wave acquisition equipment (i.e., horizontally oriented source and geophones). Ivanov et al. (2017) acquired horizontal component seismic data with the MALW method to characterize the geologic properties of levees. Comina et al. (2017) integrated Love-wave dispersion and SH seismic reflection data for V_s determination over quick clays. In many hydrologic settings, topographic variations and discontinuities of the stratigraphy influence the transport of groundwater (e.g., Miller et al. 1999). Determining the nature and locations of stratigraphic V_s anomalies with the MASW and MALW methods could be an essential part of hydrologic characterization (Konstantaki et al. 2013; Pasquet et al. 2015).

In this paper, we present a case study using both MASW and MALW to estimate the 3D V_s structure at the Boise Hydrogeophysical Research Site (BHRS). The BHRS consists of 18 wells in a shallow, unconfined aquifer near Boise, Idaho, USA, which is perfectly suitable for surface, surface-to-borehole, and cross-well geophysical field studies (e.g., Michaels and McCabe 1999; Barrash et al. 1999; Barrash and Clemo 2002; Barrash and Reboulet 2004; Clement and Knoll 2006; Moret et al. 2006; Ernst et al. 2007; Johnson et al. 2007; Bradford et al. 2009). We obtained the pseudo-3D V_s distribution with the MASW and MALW methods and delineated a low-velocity anomaly at the BHRS. We compared our results with those of borehole and ground-penetrating radar (GPR) measurements. The differences in shear-wave velocity determined by MASW, MALW, and borehole measurements are discussed.

In the following text, we first illustrate the methodologies of MASW and MALW for the reconstruction of near-surface velocity structures. Then we give a description of the Boise Hydrogeophysical Research Site and the data collection of Rayleigh and Love waves at the site. Model tests with synthetic Rayleigh-wave data were implemented before data processing to evaluate the effects of different initial models for optimized reconstruction of sharp discontinuities with strong vertical contrasts. The results of 1D, pseudo-2D, and pseudo-3D velocity structures obtained with MASW and MALW are presented and compared with the results of borehole and GPR surveys. Finally, we discuss the differences in S-wave velocities estimated by MASW, MALW, and borehole measurements and draw a conclusion that the combined use of MASW and MALW confirmed the location of the low-velocity anomaly caused by a sand channel and identified an anisotropic feature at the BHRS.

2 Multichannel Analysis of Rayleigh and Love Waves

The multichannel analysis of Rayleigh and Love waves mainly consists of three steps (Park et al. 1999; Miller et al. 1999; Xia et al. 1999, 2014):

- (1) Acquire high-frequency broadband Rayleigh/Love waves using a multichannel recording system along a linear survey line;
- (2) Extract dispersion curves from Rayleigh/Love waves; and
- (3) Invert Rayleigh/Love-wave dispersion curves to obtain near-surface 1D Vs profiles. Pseudo-2D Vs sections are constructed by aligning 1D models (Miller et al. 1999; Xia et al. 2005; Luo et al. 2009). We construct the pseudo-3D velocity structure by merging multiple 2D Vs sections from different survey lines. Therefore, additional two steps are required for creating the 3D velocity structure:
- (4) Align 1D Vs profiles to construct pseudo-2D Vs sections; and
- (5) Merge multiple 2D Vs sections to construct the pseudo-3D velocity structure.

The equipment and instruments used in surface-wave data acquisition are almost the same as used in the shallow reflection surveys except for low-frequency geophones (normally 4.5 Hz) with the aim of recording wide-bandwidth surface waves (e.g., Xia et al. 2009). Rayleigh waves can be generated by a vertical source (e.g., sledgehammers, weight drops, or vibrators) and recorded by vertical component geophones on the free surface. Love waves are generated with a horizontally oriented source and recorded by horizontal component geophones (oriented perpendicular to the survey line). Optimal data acquisition parameters are necessary to record planar Rayleigh and Love waves. The reconstructed lateral discontinuities on a final 2D Vs section are influenced by parameters of the data acquisition. The spread length of receivers that are used to extract the dispersion curve for one Vs profile sets the theoretical lower limit of horizontal resolution, because the S-wave velocity profile is an average result below the recording array (Park 2005; Xia et al. 2005; O'Neill et al. 2008; Mi et al. 2017). There are several articles discussing selections of data acquisition parameters of surface waves (e.g., Forbriger 2003; Zhang et al. 2004; O'Neill 2004; Xia et al. 2004, 2006, 2009; Xu et al. 2006, 2009).

The acquired raw data of Rayleigh/Love waves in the time-offset ($t-x$) domain are transformed to the frequency–wavenumber ($f-k$) or frequency–phase velocity ($f-v$) domain for dispersion curve extraction. Generating reliable dispersion spectra is a key step in the

MASW and MALW methods. Various algorithms such as f - k transformation (e.g., Yilmaz 1987), τ - p transformation (McMechan and Yedlin 1981), phase shift (Park et al. 1998), frequency decomposition and slant stacking (Xia et al. 2007), high-resolution linear Radon transformation (LRT, Luo et al. 2008), and generalized S-transform (Askari and Hejazi 2015) can be used to generate the dispersion image. The existence of bad traces may cause some artifacts in the dispersion energy image. Hu et al. (2018) pointed out that bad traces should be alternatively muted (zeroed) or removed (deleted) from the raw surface-wave data before dispersion imaging. Lateral heterogeneity can also cause perturbations on the observed phase velocity of surface waves (Strobbia and Foti 2006; Mi et al. 2017). To account for lateral heterogeneity, window-controlled spatial filtering (Bergamo et al. 2012; Ikeda et al. 2013) could be used to improve the dispersion measurement. These approaches were developed based on the analysis of Rayleigh waves and could be applied for Love-wave dispersion curve extraction.

The inversion of Rayleigh/Love-wave dispersion curves suffers from solution nonuniqueness. For a layered earth model, Rayleigh-wave phase velocity c_R at frequency f is determined by a characteristic equation F_R in its nonlinear, implicit form (e.g., Thomson 1950; Haskell 1953; Xia et al. 1999):

$$F_R(f, c_R, \mathbf{v}_S, \mathbf{v}_P, \boldsymbol{\rho}, \mathbf{h}) = 0 \quad (1)$$

where \mathbf{v}_S (S-wave velocity), \mathbf{v}_P (P-wave velocity), $\boldsymbol{\rho}$ (density), and \mathbf{h} (thickness of layers) are four groups of earth properties of a layered model. Love waves are independent of P-wave velocity, and the characteristic equation F_L is:

$$F_L(f, c_L, \mathbf{v}_S, \boldsymbol{\rho}, \mathbf{h}) = 0 \quad (2)$$

where c_L is Love-wave phase velocity at frequency f . Equations (1) and (2) can be solved numerically by means like the Thomson–Haskell method (Thomson 1950; Haskell 1953), the Knopoff method (Schwab and Knopoff 1972), and the reflection and transmission coefficients method (Kennett 1983; Chen 1993). Analysis of the Jacobian matrix provides a measure of phase velocity sensitivity to the earth properties (Xia et al. 1999). S-wave velocity is the dominant influence on a dispersion curve, so P-wave velocity and density are assumed known and only S-wave velocities at different depths are unknowns in inversion. In order to reduce the nonuniqueness and improve the stability and efficiency of the inversion, different algorithms have been developed, including both local (e.g., Xia et al. 1999) and global (e.g., Beaty et al. 2002; Socco and Boiero 2008; Maraschini and Foti 2010; Song et al. 2012) search methods. The iterative inversion algorithm by solving a weighted least-squares inversion problem (Xia et al. 1999) has been verified to be stable and efficient. Therefore, we used this method to invert Rayleigh/Love-wave phase velocities for S-wave velocity versus depth profiles.

3 Site Description and Data Collection

The BHRS is an experimental well field located on a gravel bar adjacent to the Boise River, 15 km from downtown Boise, Idaho, USA (Barrash et al. 1999, Fig. 1a). Deposits at this site are the youngest in a series of Pleistocene to Holocene coarse fluvial deposits, including massive coarse-gravel sheets; sheets with weak subhorizontal layering and with planar and trough cross-bedded coarse-gravel facies; and sand channels, lenses, and drapes (Jussel et al. 1994; Klingbeil et al. 1999; Heinz et al. 2003).

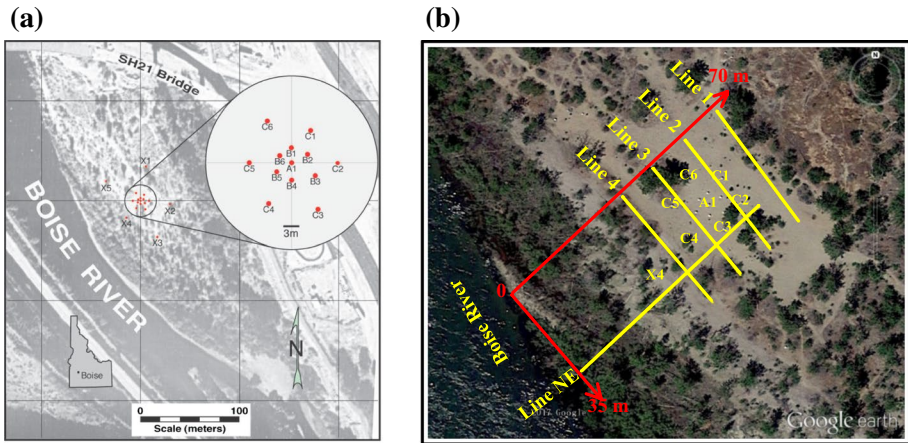


Fig. 1 a Location of the Boise Hydrogeophysical Research Site and the well field layout (Barrash et al. 1999). b The MASW and MALW survey lines

There are 18 wells in the experimental well field with 13 wells located in the central area (20 m in diameter, Fig. 1a). The wells in this central area consist of an inner ring with six wells B1–B6 roughly 3 m from A1 and an outer ring with six wells C1–C6 between 7 and 10 m from A1. There are also five boundary wells X1–X5 located 10–35 m from the central area. All of these wells were drilled to a depth of 20 m. The composition of the well field supports a wide variety of single-well, cross-well, and multiple-well hydrologic and geophysical tests for thorough three-dimensional investigation of the central area (e.g., Clement and Knoll 2006; Moret et al. 2006; Ernst et al. 2007; Johnson et al. 2007). Downhole SH-wave surveys (Michaels and McCabe 1999) present the S-wave velocities above a depth of 20 m in each well, which show this area can be roughly divided into two layers with strong velocity contrast. The V_s of the first layer is approximately 100 m/s with 2–4 m thickness and the V_s of the half-space (below 4 m depth) exceeds 500 m/s.

Five stratigraphic units have been identified in the central area of the site based on the analysis of neutron porosity logs (Barrash and Clemo 2002), grain size distributions in core samples (Barrash and Reboulet 2004), and ground-penetrating radar (GPR) measurements (Bradford et al. 2009). The youngest unit is a coarse grained, high-porosity sand channel that erodes into the unit below (Barrash and Clemo 2002). The sand channel trends northwest across the well field and is roughly parallel to the river (Bradford et al. 2009). The unit pinches out toward the northeast near the central well A1. The stratigraphic units at the BHRS have geophysical boundaries. The lateral variability in position and shape of the major unit boundaries has been defined by borehole and GPR measurements (Barrash and Clemo 2002; Barrash and Reboulet 2004; Bradford et al. 2009).

With the aim of delineating the depth and lateral variation of the major unit boundaries based on seismic S-wave velocity measurements, the MASW and MALW surveys were conducted along five different lines (Fig. 1b). Four parallel lines (Lines 1–4, each line with a length of 34.5 m, 10 m distance between adjacent lines) were located around the central area making the well A1 in the center between Lines 2 and 3. The four lines were approximately parallel to the Boise River, from the northwest to the southeast,

which were considered to be parallel to the subsurface sand channel. A cross-line (Line NE, with a length of 58.75 m) was perpendicular to Lines 1–4, for the sake of getting a NE section perpendicular to the structural trends of this area.

In the surveys along Lines 1–4, Rayleigh-wave data were collected by 24 vertical component geophones with 1.5 m spacing. The source for Rayleigh waves was a hammer vertically hitting a plate. Three shot gathers were acquired at each line with 1.5 m, 9 m, and 18 m nearest source-to-receiver offsets. For Love-wave data, the source was changed to a polarized seismic source with a hammer impacting the long dimension of a fixture (S-wave source plate) oriented perpendicular to the survey line. Love-wave data were recorded using 24 horizontal component geophones perpendicular to the survey line, with 1.5 m spacing. For each source location, two records were generated by hitting two sides of the oriented source, each with a phase difference of 180° . By subtracting these two records, noises were suppressed (Helbig 1986) and Love waves were enhanced.

For the survey along Line NE, a land streamer composed of 48 vertical component geophones and 48 horizontal component geophones (oriented perpendicular to the survey line) was used for data acquisition (Fig. 2). The geophone spacing was 1.25 m. The source had a 45° angled plate at each side (Fig. 2). This type of source is used in near-surface P- and SH-wave surveys (e.g., Uhlemann et al. 2016). With this source, Rayleigh- and Love-wave data were simultaneously acquired. By hitting each side of the source with a hammer, the vertical and horizontal (perpendicular to the survey line) components of seismic waves were recorded using the land streamer. We obtained Rayleigh and Love waves by adding two vertical component records and subtracting two horizontal component records, respectively.

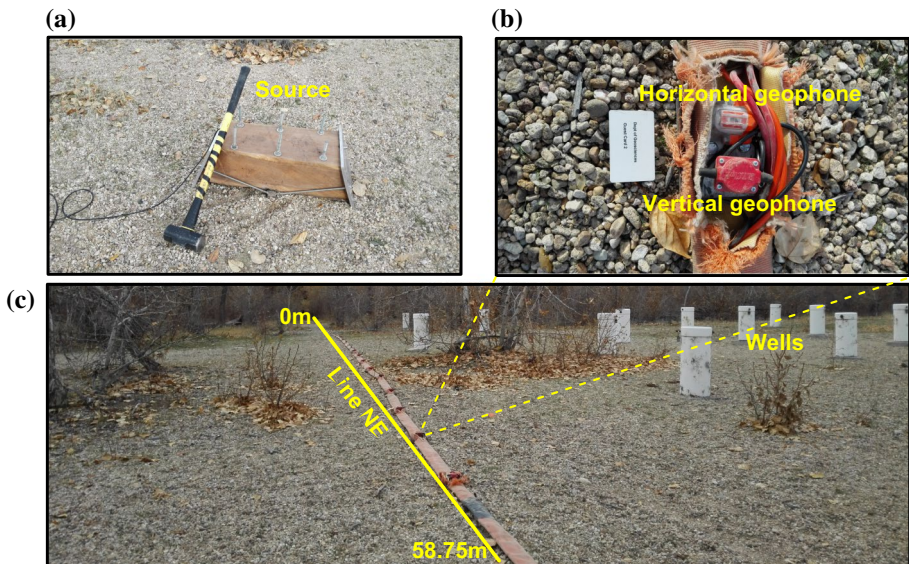


Fig. 2 Illustration of the data acquisition along Line NE. **a** The source. **b** The horizontal and vertical component geophones. **c** The land streamer

4 Synthetic Tests on the Detection of Sharp Discontinuities

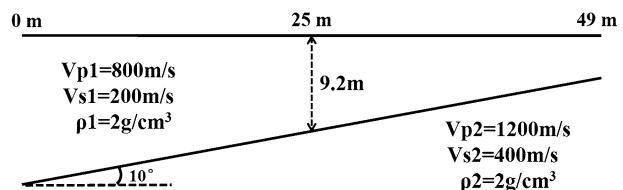
The a priori information and borehole surveys at the site suggest that sharp discontinuities exist with strong vertical contrasts in the shallow subsurface. The choice of the initial model plays an important role in the iterative inversion for the reconstruction of such discontinuities. A synthetic slope model (Fig. 3) was tested using MASW with different initial models. The simplified slope model contains sharp discontinuities (similar to the subsurface model at the BHRS, according to borehole measurements). This model can be considered as the splicing of a series of two-layer models from left to right with decreasing thickness in the first layer. We obtained the MASW Vs sections of this model using the numerical investigation procedure presented by Mi et al. (2017), which is based on the finite-difference modeling of shot gathers and then processing the synthetic data with MASW. In the modeling, the source is a 20 Hz (peak frequency) Ricker wavelet with a 60 ms delay, located at the free surface. In order to delineate the dipping interface above the depth of 15 m, 25 receivers with 1 m spacing were used for each synthetic shot gather. (The receiver spread length is 24 m, as about twice the maximum investigation depth.) The source interval is 2 m.

We tested three different initial models (Fig. 4a, c, and e) in the inversions of dispersion curves extracted from the synthetic shot gathers for 1D Vs profiles. The initial models shown in Fig. 4a, c, and e were the splicing of a series of 1D initial models at each location. All the 1D initial models were composed of fourteen layers (1 m thickness for each layer) on a half-space. The first initial model (Fig. 4a) consisted of a 1D layered model with sharp discontinuities where the velocity interface became shallower from left to right, similar to the true slope model. The second initial model (Fig. 4c) consisted of one model with sharp discontinuities and the depth of the velocity interface was constant throughout. The third initial model (Fig. 4e) included S-wave velocities increasing gradually with depth.

The corresponding pseudo-2D Vs sections were generated by aligning the inverted 1D models using a spatial interpolation scheme (Fig. 4b, d, and f). The pseudo-2D Vs section generated with the first type of initial models (Fig. 4b) presented a dipping interface with sharp discontinuities. Both the S-wave velocity and the dipping interface position were in agreement with the true model. The Vs section generated with the second type of initial models (Fig. 4d) was not accurate because neither S-wave velocities nor the position of the dipping interface was consistent with the true model. The Vs section generated with the third type of initial models (Fig. 4f) presented a smooth velocity model where the position of the dipping interface was accurately reconstructed.

Obviously, good initial models lead to more accurate inversion results for sharp discontinuities. However, for field data applications, the true subsurface model (i.e., the depth of the velocity interface) is unknown if no other a priori information is available. Based on the synthetic results, we chose smooth velocity initial models (e.g., Figure 4e) for inversion of the field data. The measured phase velocities at specific frequencies were used to define initial depth-dependent S-wave velocities (referring to Xia et al. 1999).

Fig. 3 Illustration of a synthetic model. The model contains a 10° sloping interface with a depth of 9.2 m at the location of 25 m



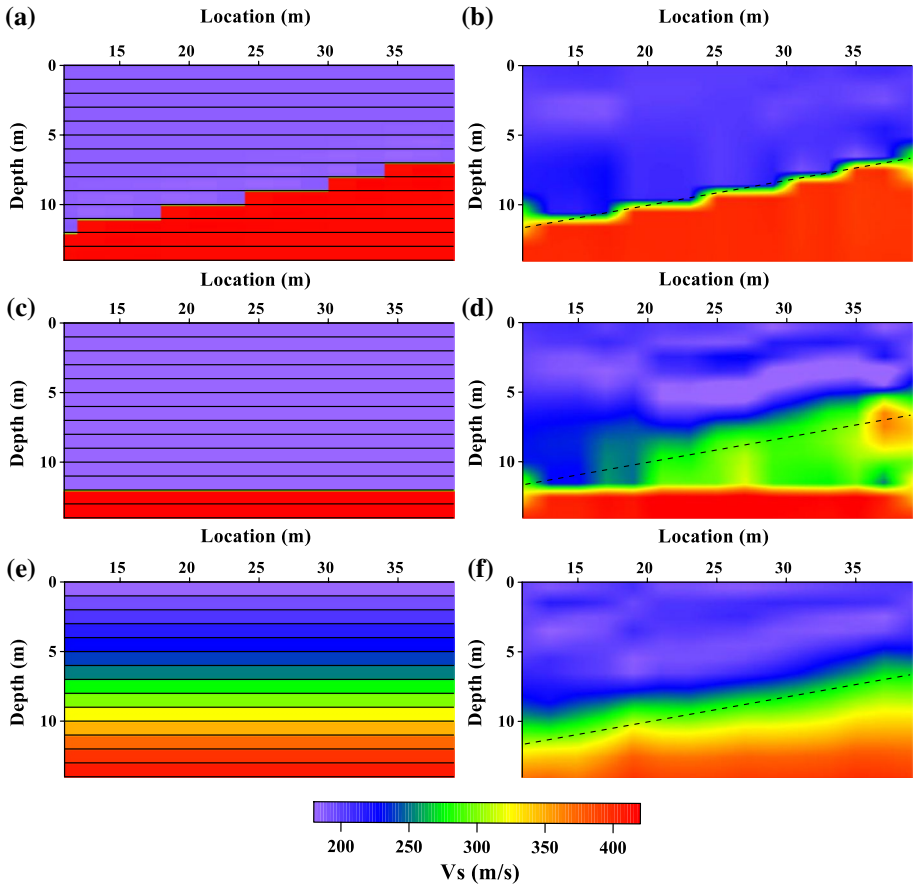


Fig. 4 Pseudo-2D Vs sections **b**, **d**, and **f** generated using the MASW method with different initial models **a**, **c**, and **e** for the slope model. The initial models are the splicing of a series of 1D initial models at each location and the pseudo-2D Vs sections are generated by aligning the inverted 1D models using a spatial interpolation scheme. The dashed lines in **b**, **d**, and **f** represent the dipping interface

5 Data Processing and Results

1D average S-wave velocity profiles were first obtained from Lines 1–4 by extracting and inverting dispersion curves of Rayleigh and Love waves using the 24 traces of each shot gather. Figure 5 shows the Rayleigh- and Love-wave data at Line 3. Dispersion images were generated with the phase shift method after removing bad traces in the shot gather to ensure their accuracy (Hu et al. 2018). “Mode kissing” was observed in Rayleigh-wave dispersion analysis, which was consistent with the results reported by Gao et al. (2016) that the “mode kissing” caused the higher mode energy at lower frequencies (<13 Hz) to be misidentified as the fundamental mode energy (Fig. 5b). Therefore, Rayleigh-wave energy trends were not picked below 13 Hz. We used a priori information and measured dispersion curves to build a smooth starting model for the inversion. The fitness of the inverted and measured dispersion curves is shown in Fig. 6. The root-mean-square (RMS) errors dropped to 7.9 m/s after three iterations for Rayleigh waves (Fig. 6b). During Love-wave

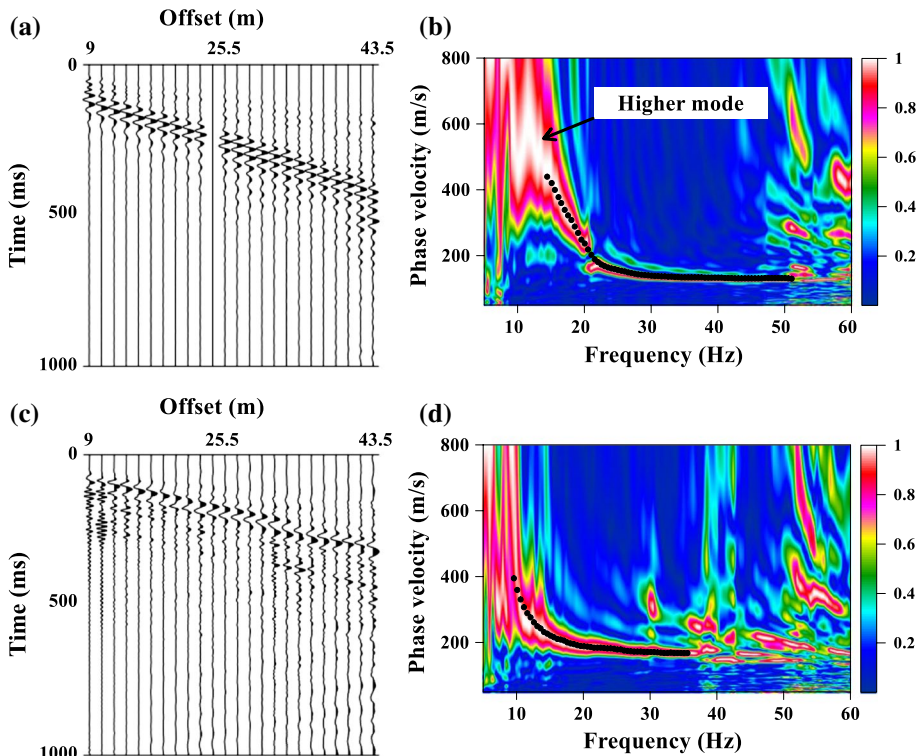


Fig. 5 **a** A Rayleigh-wave shot gather from Line 3. **b** The Rayleigh-wave dispersion image generated from **(a)**. **c** A Love-wave shot gather from Line 3. **d** The Love-wave dispersion image generated from **(c)**. Dots in **b** and **d** represent the picked fundamental dispersion curves. The color scale represents the distribution of the normalized wavefield energy in the f - v domain. There is a “mode kissing” in the Rayleigh-wave dispersion image **(b)**, and the energy at lower frequencies (> 13 Hz) is the higher mode energy (more details can be found in Gao et al. 2016)

inversion, the RMS errors decreased quickly from 31.8 m/s to 3.4 m/s within two iterations (Fig. 6d). All the RMS errors of Rayleigh- and Love-wave inversion results were below 10 m/s. The inverted 1D Vs profiles from each of Lines 1–4 (Fig. 7) highlighted the strong velocity contrast between the shallow and deep layers. S-wave velocities were less than 200 m/s between 0 and 4 m depth and then increased to more than 500 m/s below the 4 m depth. In addition, comparing the results from different lines, S-wave velocities in the shallow layer decreased gradually from Line 1 to Line 4. Furthermore, the MASW and MALW results were basically consistent with the vertical seismic profiles (VSP) obtained from the downhole SH-wave surveys (Michaels and McCabe 1999). The detailed differences in MASW, MALW, and VSP results will be discussed in the next section.

For reconstruction of 2D lateral variations, it was critical to choose relatively small quantities of traces with the optimal nearest offset to extract local dispersion curves. For a 6 m investigation depth, 7 traces were used to generate a local Rayleigh-wave dispersion image at Line NE (Fig. 8a). The local Love-wave dispersion image at Line NE (Fig. 8b) was generated with 11 traces due to some bad traces. Each local dispersion image was generated in turn with one trace updated, which meant the spatial acquisition interval of the local dispersion curves was 1.25 m. A multiple of shot

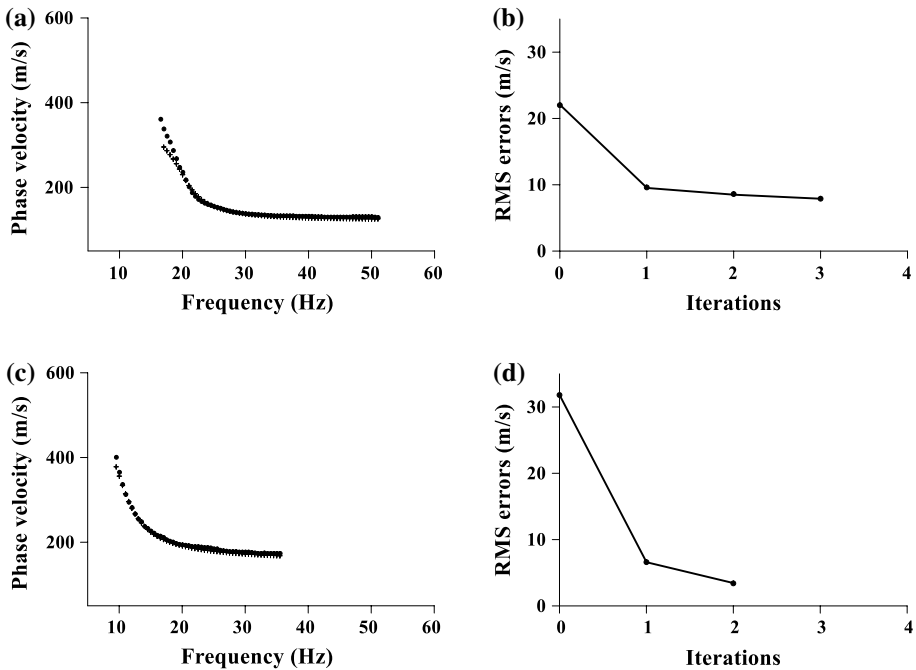


Fig. 6 **a** Measured (dots) and inverted (crosses) dispersion curves of Rayleigh waves from Line 3. **b** RMS errors of Rayleigh-wave inversion. **c** Measured (dots) and inverted (crosses) dispersion curves of Love waves from Line 3. **d** RMS errors of Love-wave inversion

gathers with different source locations (the source spacing was set to 3.75 m) were collected to keep the nearest distance of the source and selected traces around 6 to 10 m. Each dispersion curve was inverted to give a local 1D Vs profile. After inverting all the local dispersion curves, pseudo-2D Vs sections were produced using a spatial interpolation scheme (Fig. 9). The MALW Vs section is generally consistent with the Vs section of MASW. The shallow zone on the sections with S-wave velocities below 200 m/s is interpreted as the unconsolidated deposits. The low-velocity (<180 m/s) anomaly appears sunken between 20 and 45 m (locations in the horizontal direction), associated with the coarse grained, high-porosity sand channel measured by the GPR survey (Fig. 9, the water table is at approximately 2 m depth). The S-wave velocities gradually increased from 200 to 500 m/s under the sand channel.

Rayleigh- and Love-wave data from Lines 1–4 were also processed to generate 2D Vs sections. We then combined all the results from Lines 1–4 and NE to obtain the pseudo-3D Vs structure (Fig. 10). Lines 1–4 intersected Line NE and S-wave velocities matched at the intersection. We interpreted the contour line Vs=180 m/s as the bottom boundaries of the low-velocity anomaly. After a spatial interpolation scheme, we showed the 3D structure of the boundaries (Fig. 11). The low-velocity anomaly trends to the northwest and the bottom boundaries range from 1 to 4 m depth. The boundaries are deeper at the middle of the 3D structure, which corresponds to the sand channel of the field site.

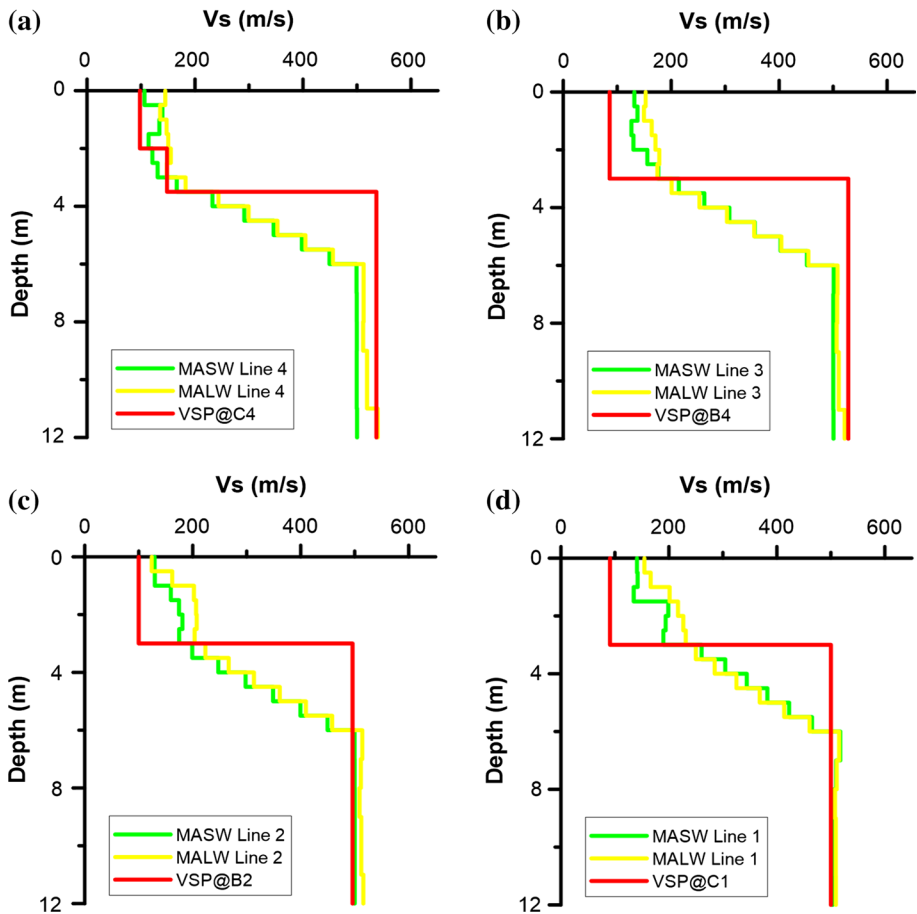


Fig. 7 Shear-wave velocity profiles at Lines 1–4 estimated by the MASW and MALW methods and comparisons with the vertical seismic profiles (VSP) from the downhole SH-wave surveys

6 Discussion

Shear-wave velocities determined by MASW and MALW have been compared with those from downhole seismic surveys (Fig. 7). The shape and position of the low-velocity anomaly estimated by MASW and MALW showed consistency with the results of borehole and GPR surveys (Fig. 9, referring to Barrash and Clemo 2002, Barrash and Reboulet 2004, and Bradford et al. 2009, in which they called the sand channel Unit 5). The downhole seismic survey results showed sharp discontinuities between the shallow and deep layers. However, this sharp velocity contrast was not observed in the MASW and MALW results. The surface-wave field data results are consistent with those of synthetic tests, in which the V_s section generated with the MASW method presents a smooth velocity model for sharp discontinuities (Fig. 4f).

We have shown that in the inversion results of MASW and MALW, the RMS errors are below 10 m/s (5%). Based on these findings, we quantitatively analyzed the differences between MASW, MALW, and VSP results at the BHRS. We calculated the relative

Fig. 8 **a** A local Rayleigh-wave dispersion image generated with 7 traces (Trace 15 to 21 at Line NE). The Rayleigh-wave bandwidth ranged from 18 to 70 Hz, which enabled the 6 m depth of investigation. **b** A local Love-wave dispersion image generated with 11 traces (Trace 15 to 25 at Line NE). Lower frequencies were obtained for Love waves (from 10 to 50 Hz). Dots in **a** and **b** represent the picked dispersion curves. The color scale represents the distribution of the normalized wavefield energy in the f - v domain

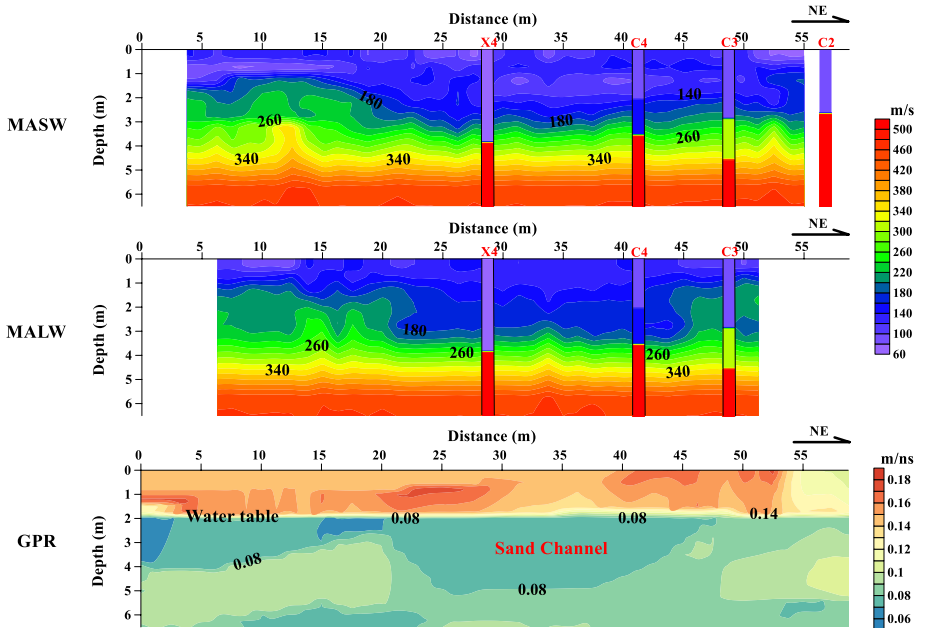
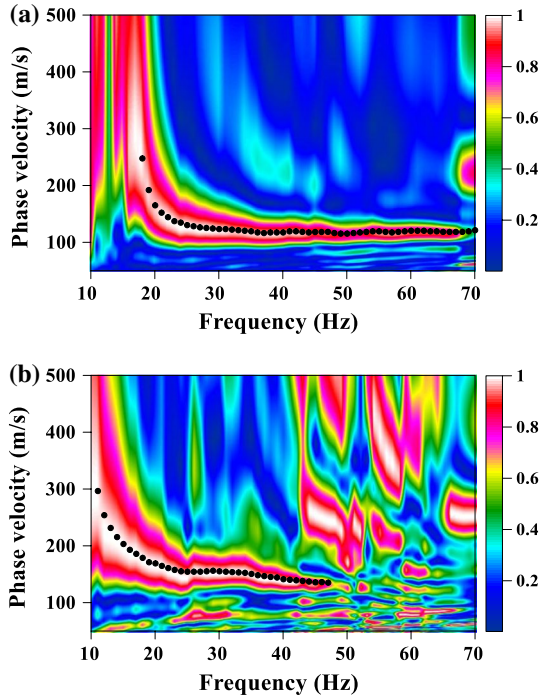


Fig. 9 Pseudo-2D Vs sections generated by the MASW and MALW methods and the GPR velocity profile at Line NE. C2, C3, C4, and X4 are the wells projected to the survey line, presenting the S-wave velocities by downhole SH-wave surveys

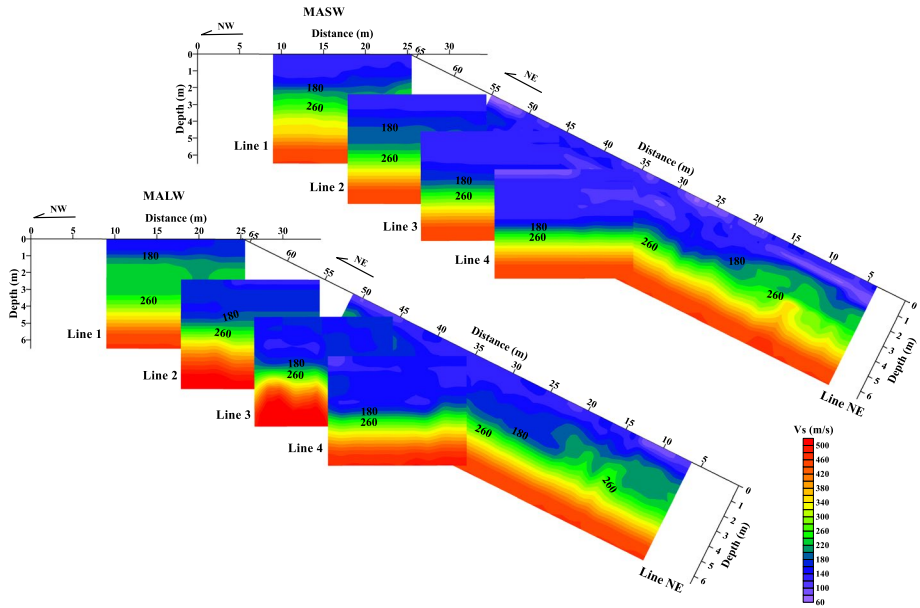


Fig. 10 Pseudo-3D Vs structures by combining Vs sections Lines 1–4 and NE

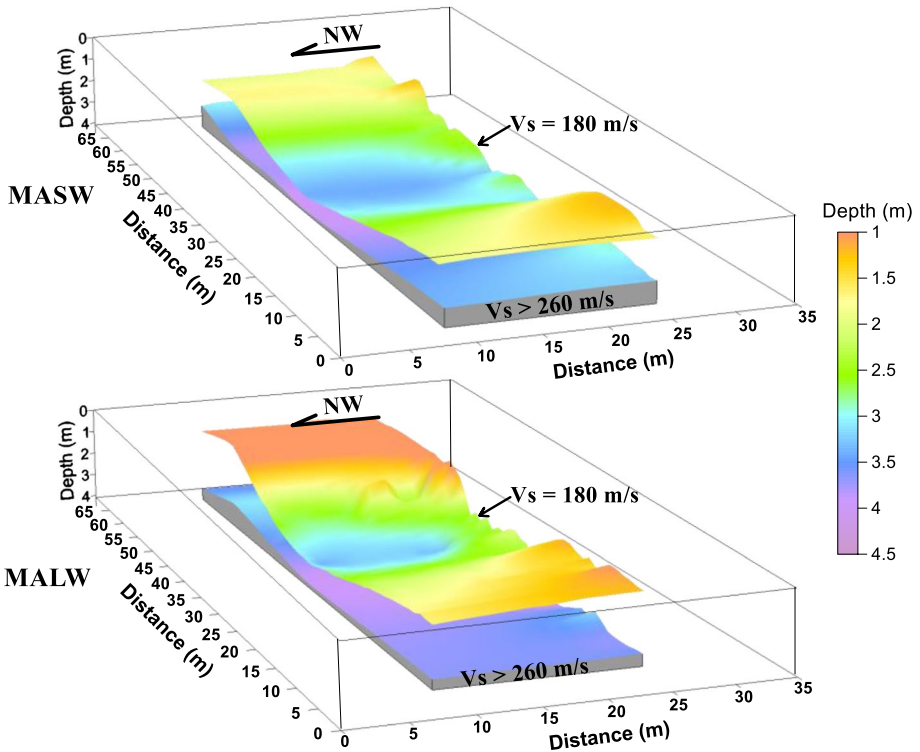


Fig. 11 3D structures at the BHRIS using the MASW and MALW surveys. The color scale represents the depth of the boundaries. The low-velocity anomaly trends to the northwest

Table 1 Relative differences of Vs above the 4 m depth at Lines 1–4 with different methods

	MALW versus MASW (%)	MASW versus VSP	MALW versus VSP
Line 4	15.86	9.73	25.47
Line 3	14.73	48.91	62.64
Line 2	14.49	43.94	57.30
Line 1	18.05	57.11	73.30

differences of S-wave velocities in the shallow layers between MASW, MALW, and VSP results as

$$\eta = \frac{2(V_{S1} - V_{S2})}{V_{S1} + V_{S2}} \times 100\%, \quad (3)$$

where V_{S1} and V_{S2} represented the S-wave velocities estimated by two different methods. S-wave velocities estimated from surface waves are greater than those from downhole SH-wave surveys (Table 1). The differences in Vs from MASW/MALW and VSP exceed 15%, a value quoted in a previous study by comparing MASW results and direct borehole Vs logging measurements (Xia et al. 2002), which may indicate anisotropy in the horizontal and vertical directions at the BHRS. Also estimation errors associated with the shallow velocity layer from the VSP surveys may account for the large differences in Vs between MALW and VSP results. S-wave velocities estimated by MALW are approximately 15% greater than those from MASW (Table 1), suggesting a positive radial anisotropy ($V_{SH} > V_{SV}$) in the shallow layer at the BHRS. The anisotropy at the BHRS may be caused by the thin layering within sedimentary materials or the orientation of the crystals in the medium associated with groundwater flow.

7 Conclusions

We present a case study using multichannel analysis of Rayleigh and Love waves to estimate the shallow 3D structures at the Boise Hydrogeophysical Research Site. Shear-wave velocity structures obtained by both MASW and MALW were consistent with the results of previous borehole and ground-penetrating radar measurements. The lateral variability in position and shape of the low-velocity anomaly associated with a sand channel was delineated at the meter scale. The MASW and MALW methods provided smooth velocity structures where Vs gradually increased with depth even though a sharp, high-velocity contrast was observed in the downhole seismic results. The large differences between surface-wave and VSP results in the shallow velocity layer could be due to estimation errors from the VSP surveys. The differences in shear-wave velocities determined by MASW and MALW were around 15% and suggested the positive radial anisotropy ($V_{SH} > V_{SV}$) at the BHRS in the shallow layer. The combined use of MALW and MASW can be a powerful tool for near-surface characterization.

Acknowledgements The authors greatly appreciate the comments and suggestions from the Editor in Chief Michael J. Rycroft and two anonymous reviewers that significantly improved the quality of the manuscript. The authors thank the staff and students in the Center for Geophysical Investigation of the Shallow Subsurface (CGISS), Boise State University, for their generous help in data acquisitions. The VSP data are from

the borehole report by P. Michaels and P.E.J. McCabe. The first author thanks Prof. Laura Valentina Socco for helpful discussions on this research. This study is supported by the National Natural Science Foundation of China (NSFC) under Grant Nos. 41774115 and 41830103 and the China Postdoctoral Science Foundation under Grant No. 2019M652061.

References

- Anderson D (1961) Elastic wave propagation in layered anisotropic media. *J Geophys Res* 66(9):2953–2963
- Askari R, Hejazi SH (2015) Estimation of surface-wave group velocity using slant stack in the generalized S-transform domain surface-wave group velocity estimation. *Geophysics* 80(4):EN83–EN92
- Barrash W, Clemo T (2002) Hierarchical geostatistics and multifacies systems: Boise Hydrogeophysical Research Site, Boise, Idaho. *Water Resour Res* 38(10):1196
- Barrash W, Reboulet EC (2004) Significance of porosity for stratigraphy and textural composition in subsurface coarse fluvial deposits: Boise Hydrogeophysical Research Site. *Geol Soc Am Bull* 116(9/10):1059–1073
- Barrash W, Clemo T, Knoll MD (1999) Boise Hydrogeophysical Research Site (BHRS): objectives, design, initial geostatistical results, paper presented at symposium on the application of geophysics to environmental and engineering problems 1999. Environmental and Engineering Geophysical Society, Oakland
- Beaty KS, Schmitt DR, Sacchi M (2002) Simulated annealing inversion of multimode Rayleigh wave dispersion curves for geological structure. *Geophys J Int* 151:622–631
- Bergamo P, Boiero D, Socco LV (2012) Retrieving 2D structures from surface-wave data by means of space-varying spatial windowing. *Geophysics* 77(4):EN39–EN51
- Boaga J, Cassiani G, Strobbia CL, Vignoli G (2013) Mode misidentification in Rayleigh waves: ellipticity as a cause and a cure. *Geophysics* 78(4):EN17–EN28
- Boiero D, Socco LV (2010) Retrieving lateral variations from surface wave dispersion curves analysis. *Geophys Prospect* 58(6):977–996
- Bradford JH, Clement WP, Barrash W (2009) Estimating porosity with ground-penetrating radar reflection tomography: a controlled 3-D experiment at the Boise Hydrogeophysical Research Site. *Water Resour Res* 45:W00D26
- Chen X (1993) A systematic and efficient method of computing normal modes for multilayered half-space. *Geophys J Int* 115:391–409
- Cheng C, Chen L, Yao H, Jiang M, Wang B (2013) Distinct variations of crustal shear wave velocity structure and radial anisotropy beneath the North China Craton and tectonic implications. *Gondwana Res* 23(1):25–38
- Clement WP, Knoll MD (2006) Traveltime inversion of vertical radar profiles. *Geophysics* 71:K67–K76
- Comina C, Krawczyk CM, Polom U, Socco LV (2017) Integration of SH seismic reflection and Love-wave dispersion data for shear wave velocity determination over quick clays. *Geophys J Int* 210(3):1922–1931
- Dal Moro G, Moura RM, Moustafa SR (2015) Multi-component joint analysis of surface waves. *J Appl Geophys* 119:128–138
- Ernst JR, Green AG, Maurer H, Holliger K (2007) Application of a new 2-D time-domain full-waveform inversion scheme to crosshole radar data. *Geophysics* 72(5):J53–J64
- Fiore VD, Cavuoto G, Tarallo D, Punzo M, Evangelista L (2016) Multichannel analysis of surface waves and down-hole tests in the archeological “palatine hill” area (rome, italy): evaluation and influence of 2D effects on the shear wave velocity. *Surv Geophys* 37(3):625–642
- Forbriger T (2003) Inversion of shallow-Seismic wavefields: I wavefield transformation. *Geophys J Int* 153(3):719–734
- Foti S, Parolai S, Albarello D, Picozzi M (2011) Application of surface-wave methods for seismic site characterization. *Surv Geophys* 32:777–825
- Gao L, Xia J, Pan Y, Xu Y (2016) Reason and condition for mode kissing in MASW method. *Pure Appl Geophys* 173(5):1627–1638
- Garofalo F, Foti S, Hollender F, Bard P, Cornou C, Cox BR, Dechamp A, Ohrnberger M, Perron V, Sicilia D, Teague D, Vergniault C (2016) InterPACIFIC project: comparison of invasive and non-invasive methods for seismic site characterization. Part II: inter-comparison between surface-wave and borehole methods. *Soil Dyn Earthq Eng* 82:241–254
- Haskell NA (1953) The dispersion of surface waves on multilayered media. *Bull Seismol Soc Am* 43:17–34
- Hayashi K, Suzuki H (2004) CMP cross-correlation analysis of multichannel surface-wave data. *Explor Geophys* 35:7–13

- Heinz J, Kleineidam S, Teutsch G, Aigner T (2003) Heterogeneity patterns of quaternary glaciofluvial gravel bodies (SW-Germany): applications to hydrogeology. *Sed Geol* 158:1–23
- Helbig K (1986) Shear-wave—what they are and how they can be used. In: Danbom SH, Domenico SN (eds) *Shear-wave exploration*. Society of Exploration Geophysicists, Tulsa, pp 19–36
- Hu Y, Xia J, Mi B, Cheng F, Shen C (2018) A pitfall of muting and removing bad traces in surface-wave analysis. *J Appl Geophys* 153:136–142
- Ikeda T, Tsuji T, Matsuoka T (2013) Window-controlled CMP crosscorrelation analysis for surface waves in laterally heterogeneous media. *Geophysics* 78(6):EN95–EN105
- Ikeda T, Matsuoka T, Tsuji T, Nakayama T (2015) Characteristics of the horizontal component of Rayleigh waves in multimode analysis of surface waves. *Geophysics* 80(1):EN1–EN11
- Ivanov J, Miller RD, Lacombe P, Johnson CD, Lane JW Jr (2006) Delineating a shallow fault zone and dipping bedrock strata using multichannel analysis of surface waves with a land streamer. *Geophysics* 71(5):A39–A42
- Ivanov J, Miller RD, Feigenbaum D, Morton SLC, Peterie SL, Dunbar JB (2017) Revisiting levees in southern Texas using love-wave multichannel analysis of surface waves with the high-resolution linear Radon transform. *Interpretation* 5(3):T287–T298
- Johnson TC, Routh PS, Barrash W, Knoll MD (2007) A field comparison of Fresnel zone and ray-based GPR attenuation-difference tomography for time-lapse imaging of electrically anomalous tracer or contaminant plumes. *Geophysics* 72(2):G21–G29
- Jussel P, Stauffer F, Dracos T (1994) Transport modeling in heterogeneous aquifers: 1 statistical description and numerical generation. *Water Resour Res* 30(6):1803–1817
- Kennett BLN (1983) *Seismic wave propagation in stratified media*. Cambridge University Press, New York
- Klingbeil R, Kleineidam S, Aspiron U, Aigner T, Teutsch G (1999) Relating lithofacies to hydrofacies: outcrop-based hydrogeological characterization of Quaternary gravel deposits. *Sed Geol* 129:299–310
- Konstantaki LA, Carpentier SFA, Garofalo F, Bergamo P, Socco LV (2013) Determining hydrological and soil mechanical parameters from multichannel surface-wave analysis across the Alpine Fault at Incheon, New Zealand. *Near Surf Geophys* 11:435–448
- Lin C, Lin C (2007) Effect of lateral heterogeneity on surface wave testing: numerical simulations and a countermeasure. *Soil Dyn Earthq Eng* 27(6):541–552
- Lin F, Moschetti M, Ritzwoller M (2008) Surface wave tomography of the western United States from ambient seismic noise: Rayleigh and Love wave phase velocity maps. *Geophys J Int* 173:281–298
- Lin CP, Lin CH, Chien CJ (2017) Dispersion analysis of surface wave testing: sASW versus MASW. *J Appl Geophys* 143:223–230
- Luo Y, Xia J, Miller RD, Xu Y, Liu J, Liu Q (2008) Rayleigh-wave dispersive energy imaging by high-resolution linear Radon transform. *Pure Appl Geophys* 165(5):903–922
- Luo Y, Xia J, Liu J, Xu Y, Liu Q (2009) Research on the MASW middle-of-the-spread-results assumption. *Soil Dyn Earthq Eng* 29:71–79
- Luo Y, Xu Y, Yang Y (2013) Crustal radial anisotropy beneath the Dabie orogenic belt from ambient noise tomography. *Geophys J Int* 195(2):1149–1164
- Maraschini M, Foti S (2010) A Monte Carlo multimodal inversion of surface waves. *Geophys J Int* 182:1557–1566
- McMechan GA, Yedlin MJ (1981) Analysis of dispersive waves by wave field transformation. *Geophysics* 46:869–874
- Mi B, Xia J, Xu Y (2015) Finite-difference modeling of SH-wave conversions in shallow shear-wave refraction surveying. *J Appl Geophys* 119:71–78
- Mi B, Xia J, Shen C, Wang L, Hu Y, Cheng F (2017) Horizontal resolution of multichannel analysis of surface waves. *Geophysics* 82(3):EN51–EN66
- Mi B, Xia J, Shen C, Wang L (2018) Dispersion energy analysis of Rayleigh and Love waves in the presence of low-velocity layers in near-surface seismic surveys. *Surv Geophys* 39(2):271–288
- Mi B, Hu Y, Xia J, Socco LV (2019) Estimation of horizontal-to-vertical spectral ratios (ellipticity) of Rayleigh waves from multistation active-seismic records. *Geophysics* 84(6):EN81–EN92
- Michaels P, McCabe PEJ (1999) Interim URISP report 10: down-hole seismic surveys SH- and P- Waves. Technical Report, Boise State University Center for Geophysical Investigation of the Shallow Subsurface, pp 99–03, 08 June, 1999, Boise, Idaho
- Miller RD, Xia J, Park CB, Ivanov J (1999) Multichannel analysis of surface waves to map bedrock. *Lead Edge* 18:1392–1396
- Moret GJM, Knoll MD, Barrash W, Clement WC (2006) Investigating the stratigraphy of an alluvial aquifer using crosswell seismic traveltimes tomography. *Geophysics* 71:B63–B73
- Muyzert E, Snieder R (2000) An alternative parameterization for surface waves in a transverse isotropic medium. *Phys Earth Planet Inter* 118(1–2):125–133

- Nazarian S, Stokoe II KH (1984) In situ shear wave velocities from spectral analysis of surface waves. In: 8th conference on earthquake engineering, vol 3, pp 31–38
- Ning L, Dai T, Wang L, Yuan S, Pang J (2018) Numerical investigation of Rayleigh-wave propagation on canyon topography using finite-difference method. *J Appl Geophys* 159:350–361
- O'Neill A (2004) Shear velocity model appraisal in shallow surface wave inversion. Proceedings of ISC-2 on geotechnical and geophysical site characterization, Viana da Fonseca A, Mayne PW (eds), Millpress, Rotterdam, pp 539–546
- O'Neill A, Campbell T, Matsuoka T (2008) Lateral resolution and lithological interpretation of surface-wave profiling. *Lead Edge* 27:1550–1553
- Pan Y, Gao L, Bohlen T (2019) High-resolution characterization of near-surface structures by surface-wave inversions: from dispersion curve to full waveform. *Surv Geophys* 40(2):167–195
- Park CB (2005) MASW horizontal resolution in 2D shear-velocity (V_s) mapping. Kansas Geological Survey Open-file Report, p 4
- Park CB, Miller RD, Xia J (1998) Imaging dispersion curves of surface waves on multi-channel record. Technical program with biographies, SEG, 68th annual meeting, New Orleans, Louisiana, pp 1377–1380
- Park CB, Miller RD, Xia J (1999) Multi-channel analysis of surface waves (MASW). *Geophysics* 64:800–808
- Pasquet S, Bodet L, Dhemaied A, Mouhri A, Vitale Q, Rejiba F, Flipo N, Guérin R (2015) Detecting different water table levels in a shallow aquifer with combined P-, surface and SH-wave surveys: insights from VP/VS or Poisson's ratios. *J Appl Geophys* 113:38–50
- Qiu X, Wang Y, Wang C (2019) Rayleigh-wave dispersion analysis using complex-vector seismic data. *Near Surf Geophys* 17:487–499
- Schwab FA, Knopoff L (1972) Fast surface wave and free mode computations. In: Bolt BA (ed) *Methods in computational physics*. Academic Press, Cambridge, pp 87–180
- Schwenk JT, Sloan SD, Ivanov J, Miller RD (2016) Surface-wave methods for anomaly detection. *Geophysics* 81(4):EN29–EN42
- Sheriff RE (2002) *Encyclopedic dictionary of applied geophysics*, 4th edn. Society of Exploration Geophysicists, Tulsa
- Sloan SD, Peterie SL, Miller RD, Ivanov J, Schwenk JT, McKenna JR (2015) Detecting clandestine tunnels using near-surface seismic techniques. *Geophysics* 80(5):EN127–EN135
- Socco LV, Strobbia CL (2003) Extensive modeling to study surface wave resolution. In: Proceedings of the 16th symposium on the application of geophysics to engineering and environmental problems (SAGEEP), pp 1312–1319
- Socco LV, Boiero D (2008) Improved Monte Carlo inversion of surface wave data. *Geophys Prospect* 56:357–371
- Socco LV, Foti S, Boiero D (2010) Surface-wave analysis for building near-surface velocity models—established approaches and new perspectives. *Geophysics* 75(5):A83–A102
- Song YY, Castagna JP, Black RA, Knapp RW (1989) Sensitivity of near-surface shear-wave velocity determination from Rayleigh and Love waves. Technical program with biographies, SEG, 59th Annual Meeting, Dallas, TX, pp 509–512
- Song X, Li T, Lv X, Fang H, Gu H (2012) Application of particle swarm optimization to interpret Rayleigh wave dispersion curves. *J Appl Geophys* 84:1–13
- Strobbia C, Foti S (2006) Multi-offset phase analysis of surface wave data (MOPA). *J Appl Geophys* 59:300–313
- Thomson WT (1950) Transmission of elastic waves through a stratified solid medium. *J Appl Phys* 21:89–93
- Uhlemann S, Hagedorn S, Dashwood B, Maurer H, Gunn D, Dijkstra T, Chambers J (2016) Landslide characterization using P- and S-wave seismic refraction tomography—the importance of elastic moduli. *J Appl Geophys* 134:64–76
- Vignoli G, Strobbia C, Cassiani G, Vermeer P (2011) Statistical multi-offset phase analysis for surface wave processing in laterally varying media. *Geophysics* 76(2):U1–U11
- Wang L, Xu Y, Luo Y (2015) Numerical investigation of 3D multichannel analysis of surface wave method. *J Appl Geophys* 119:156–169
- Xia J (2014) Estimation of near-surface shear-wave velocities and quality factors using multichannel analysis of surface-wave methods. *J Appl Geophys* 103:140–151
- Xia J, Miller RD, Park CB (1999) Estimation of near-surface shear-wave velocity by inversion of Rayleigh wave. *Geophysics* 64:691–700
- Xia J, Miller RD, Park CB, Hunter JA, Harris JB, Ivanov J (2002) Comparing shear-wave velocity profiles from multichannel analysis of surface wave with borehole measurements. *Soil Dyn Earthq Eng* 22(3):181–190

- Xia J, Miller RD, Park CB, Tian G (2003) Inversion of high frequency surface waves with fundamental and higher modes. *J Appl Geophys* 52(1):45–57
- Xia J, Chen C, Li PH, Lewis MJ (2004) Delineation of a collapse feature in a noisy environment using a multichannel surface wave technique. *Geotechnique* 54(1):17–27
- Xia J, Chen C, Tian G, Miller RD, Ivanov J (2005) Resolution of high-frequency Rayleigh-wave data. *J Environ Eng Geophys* 10(2):99–110
- Xia J, Xu Y, Chen C, Kaufmann RD, Luo Y (2006) Simple equations guide high-frequency surface-wave investigation techniques. *Soil Dyn Earthq Eng* 26(5):395–403
- Xia J, Xu YX, Miller RD (2007) Generating image of dispersive energy by frequency decomposition and slant stacking. *Pure Appl Geophys* 164(5):941–956
- Xia J, Miller RD, Xu Y, Luo Y, Chen C, Liu J, Ivanov J, Zeng C (2009) High-frequency Rayleigh-wave method. *J Earth Sci* 20(3):563–579
- Xia J, Xu Y, Luo Y, Miller RD, Cakir R, Zeng C (2012) Advantages of using multichannel analysis of Love waves (MALW) to estimate near-surface shear-wave velocity. *Surv Geophys* 33(5):841–860
- Xu Y, Xia J, Miller RD (2006) Quantitative estimation of minimum offset for multichannel surface-wave survey with actively exciting source. *J Appl Geophys* 59(2):117–125
- Yilmaz O (1987) *Seismic data processing*. Society of Exploration Geophysicists, Tulsa
- Yilmaz Ö, Eser M, Berilgen M (2006) A case study of seismic zonation in municipal areas. *Lead Edge* 25:319–330
- Yin X, Xu H, Wang L, Hu Y, Shen C, Sun S (2016) Improving horizontal resolution of high-frequency surface-wave methods using travel-time tomography. *J Appl Geophys* 126:42–51
- Yuan K, Beghein C (2014) Three-dimensional variations in Love and Rayleigh wave azimuthal anisotropy for the upper 800 km of the mantle. *J Geophys Res Solid Earth* 119(4):3232–3255
- Zhang SX, Chan LS (2003) Possible effects of misidentified mode number on Rayleigh wave inversion. *J Appl Geophys* 53:17–29
- Zhang SX, Chan LS, Xia J (2004) The selection of field acquisition parameters for dispersion images from multichannel surface wave data. *Pure Appl Geophys* 161:185–201

Publisher's Note Springer Nature remains neutral with regard to jurisdictional claims in published maps and institutional affiliations.